

Contributions to Dielectric Constant Enhancement in Thin-Film Metal-Insulator-Metal

D.S. Krueger^{*1}, Z.J. Legenzoff¹, J.A. Wolf¹,
J.B. Claypool², R.W. Schwartz², W. Huebner²

¹The Department of Energy's Kansas City National Security
Campus, managed by Honeywell – Kansas City, MO

²Missouri University of Science and Technology – Rolla, MO

received January 25, 2021; received in revised form December 27, 2021; accepted January 13, 2022

Abstract

Thin-film metal-insulator-metal capacitors were fabricated with varying dielectric and electrode thicknesses and areas. Measurement of the dielectric properties of the capacitors consistently yielded higher than predicted capacitance values, which prompted the exploration of three factors that could enhance the capacitance. Modeling of the fringing capacitance and field enhancement due to the capacitor geometry, both yield capacitance gains, albeit insufficient to fully explain the observed behavior. The possible role of changes in polarizability of the dielectric film constituents, due to the amorphous nature of the films, was also evaluated, but the results of the investigation of this contribution were inconclusive. The role of accumulation/depletion layers on capacitance enhancement was also analyzed. For capacitors fabricated with thinner dielectrics, the presence of these layers can effectively reduce the dielectric thickness, resulting in contributions to capacitance that are significant. The calculations completed suggest these contributions may be more important than fringing field contributions. Additional studies of these mechanisms are in progress.

Keywords: Thin film capacitor, fringe field capacitance, dielectric enhancement

I. Introduction

(1) Thin-film capacitors on LTCC substrates

Thin-film capacitors fabricated on low-temperature-cofired ceramic (LTCC) substrates are of interest for reducing the number of solder joints and discrete components for high-density multichip modules (MCMs) and incorporation into glass interposers¹⁻³. In this work, thin-film metal-insulator-metal capacitors have been developed with varying electrode and dielectric compositions for application frequencies up to 15 MHz. The capacitors also have varying thickness and area in order to achieve specified capacitance values between 10 pF and 10 nF. Dielectric materials were selected for their stable and predictable dielectric constant and high breakdown strengths that allow operation of thin devices at fields approaching 10^6 V/cm.

While the overall research included a larger set of materials, the dielectric utilized in this study was Al_2O_3 . Polycrystalline Al_2O_3 is a linear dielectric with a dielectric constant of ~ 9.8 . Combined with its electrical resistivity $>10^{12}$ Ω cm, this makes Al_2O_3 desirable for capacitor applications that require exposure to elevated temperatures and voltage. In thin-film form, capacitance values of interest can be achieved with dielectric constants ≤ 10 , making these materials suitable choices for many development efforts.

* Corresponding author: dkrueger@kcncs.doe.gov

However, in this work nearly all experimental samples exhibited higher than predicted, or enhanced, capacitance values. Potential contributions to the enhanced capacitance include: (i) fringe effect capacitance; (ii) polarizability changes due to the amorphous structure of the materials; and (iii) the presence of accumulation or inversion layers in the dielectric layers, resulting in effectively thinner dielectric layers. These contributions have been studied individually and previously have been thought to be minor contributions, and therefore, of minimal use to consider for devices of the size and capacitance studied here. However, as the operational frequencies of capacitors have increased to 50–100 GHz and beyond, these contributions can minimize insertion losses, and therefore their usefulness has increased⁴. Understanding the contributions to the apparent enhancement of capacitance may facilitate more accurate predictive models of such devices in new higher-frequency applications.

(2) Fringe field contributions to capacitance

For a dielectric under bias, electric field lines extend beyond the geometry of the electrodes through the surrounding medium, be that air or an encapsulant. The relative magnitude of this contribution will depend upon the dielectric constant, K , of the dielectric and the surrounding medium, the geometry of the electrode edge, and the overall size of the capacitor. For the latter, smaller capac-

itors exhibit a relatively larger fringe effect as the ratio of the capacitor perimeter to the area increases.

In semiconductors and circuit design, fringe capacitance can lead to parasitic and undesirable performance, however, in discrete devices it can be used to engineer enhanced performance⁴. Accurately understanding and characterizing the extent of fringe capacitance has been studied through empirical methods and basic experiments^{5–7}. For example, Subramanian *et al.*⁸ developed the following Eq. 1 to empirically account for the fringe capacitance contribution, where the edge capacitance contribution, C_e , is a function of the capacitor perimeter, P , and the dielectric thickness, t .

$$C_e = [0.019 \ln(P/t) - 0.043]P \quad (1)$$

However, little work has been published that utilizes modern physics-based modeling tools to evaluate factors that contribute to, and can therefore be used to predict and engineer the extent of fringe capacitance within specific devices. In this study, the fringe field capacitance was calculated using 3D electromagnetic analysis software by applying physics-based calculations.

(3) Polarizability contributions to capacitance

Thin-film dielectrics are typically amorphous, and as such, they can certainly exhibit dielectric constants significantly different from crystalline systems of the same composition. Intuitively, the lower density of an amorphous system should lead to a lower K , simply due to the lower density of charged species in the material associated with increased atomic spacing. However, this assumes the ionic polarizability is constant. The more open structure of an amorphous system could lead to higher ionic displacements under field application. For example, Shannon *et al.*⁹ observed that the greater molar volume of glasses and amorphous phases, compared to crystalline compounds of identical compositions, led to an abnormal positive deviation of the dielectric constant. They postulated that the “rattling” of loosely bound cations and disordered oxygen anions contributed to the enhancement. Given these different possible contributions to the dielectric constant, determining the effects of amorphicity on contributions to capacitance was a second goal of this study. The dielectric polarizability, consisting of both ionic and electronic polarizabilities, has long been estimated for crystalline materials using the Clausius-Mossotti equation, and that approach is used in this work to explore contributions of polarizability to the observed dielectric constant.

(4) Accumulation and inversion layer contributions to capacitance

Calculation of the dielectric constant from the capacitance value incorporates the dielectric thickness; for thin-film capacitors this is typically measured directly using a profilometer. Yet this basic assumption may be incorrect if the effective dielectric thickness is actually less due to the formation of semiconducting accumulation or inversion layers within the dielectric immediately adjacent to the electrode. In the world of semiconductors, it is well known that these layers form between two materials in contact with each other due to differences in the work function.

Estimations of the relative impact of this effect are provided in this work.

II. Experimental

(1) Capacitor fabrication and characterization

A series of thin-film Al_2O_3 capacitors with Al electrodes was fabricated on DuPont 951 LTCC substrates using sputter deposition through physical “shadow” masks. As shown in Fig. 1, each substrate consisted of 48 capacitors designed with electrode widths of 150, 375, 530, and 750 μm , yielding active areas of approximately 0.0225 to 0.5625 mm^2 . There are 16 different electrode configurations in this layout, with 10 different capacitor areas. The parallel plate capacitors were fabricated with a targeted bottom metal electrode of 500 nm thickness, Al_2O_3 dielectric of 1000 nm thickness, and a top metal electrode of 500 nm thickness. Metal electrode layers were deposited from 99.99 % pure metal targets at 300 W using a DC magnetron power supply. The Al_2O_3 dielectric was deposited from a 99.9 % pure ceramic target at 200 W using an RF power supply. All materials were deposited with a Denton (Moorestown, NJ) Discovery 18 sputter deposition system using an atmosphere of 99.999 % pure Ar at a working pressure of 5–8 mtorr. No substrate heating was used during deposition. Variations in electrode width due to shadowing, and dielectric thicknesses due to process variations, were accounted for by making lateral and thickness measurements of all capacitors using a KLA Tencor (Milpitas, CA) P-17 profilometer system. A representative dimensional measurement is shown in Fig. 2.

Dielectric characterization was performed in a Faraday cage using a Hewlett Packard (Santa Clara, CA) 4194A Impedance Analyzer at 1 kHz, 10 kHz, and 100 kHz at room temperature. Though not reported in this work, capacitors fabricated using these processes have also been characterized up to 50 GHz¹⁰.

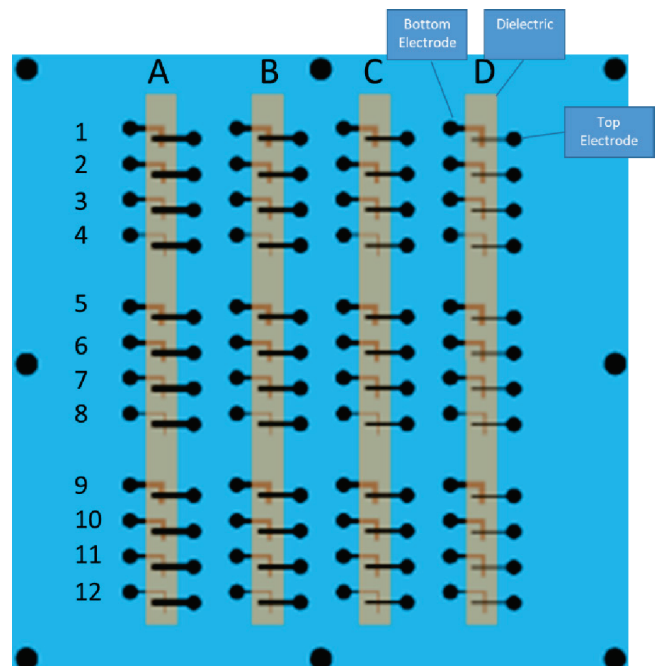


Fig. 1: Schematic layout of thin film capacitors on LTCC substrate.

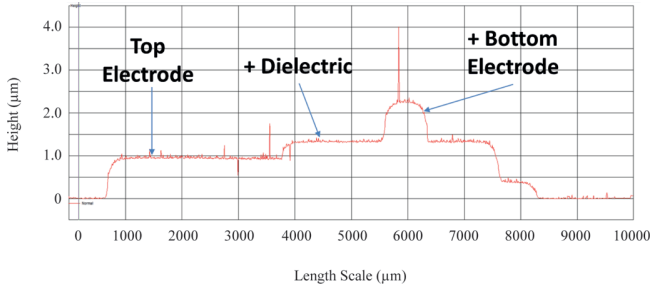


Fig. 2: Typical KLA Tencor P-17 thickness profile.

(2) Modeling of fringe field effects and fringe field capacitance

In this study, models were developed that approximate the physical structure of the as-fabricated devices to account for observed tapering of the electrode and dielectric layers. Tapering of the layers is a result of the use of a physical “shadow” mask and physical vapor deposition.

Models were developed for the capacitor devices using CST Microwave Studio (3DS Dassault Systemes) using the electrostatic solver in which the capacitor dimensions for the models utilized the defined physical mask dimensions. Perfect electrical conductors (PECs) were used for the top and bottom electrodes with the dielectric material between the two electrodes. The simulation model is shown in Fig. 3 and simulations were carried out where the capacitor was placed on an LTCC substrate with a $K = 7.8$.

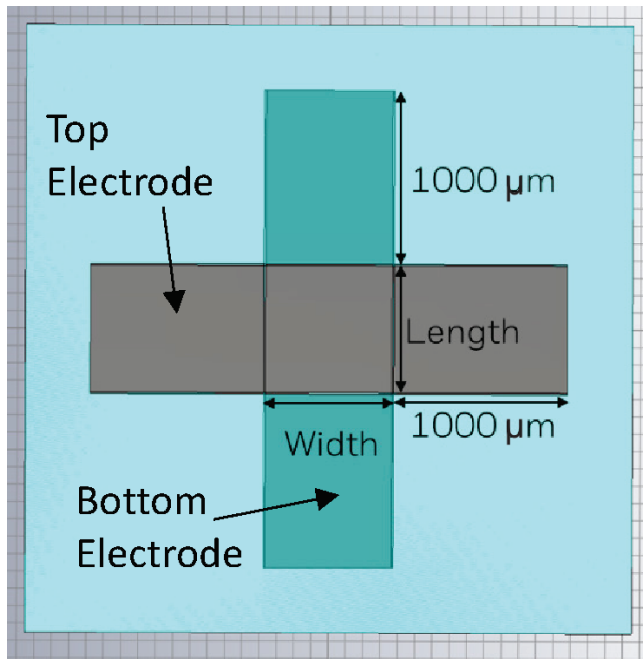


Fig. 3: Model diagram 1 (note: the aqua color is the dielectric layer).

Tapers were added to the edges of all dielectric and electrode layers, however, only the taper of the electrodes impacted the model calculations since the dielectric taper was outside of the active device area. The dielectric followed the contour of the bottom electrode taper, as shown in Fig. 4. The tapered devices have the same overall active area as the non-tapered. The taper starts 10, 100, 200, or 300 µm from the edge of the nominal dimensions. Tapering was added to the edge of electrodes as illustrated in Fig. 4

and Fig. 5, and the dielectric layer followed the contour of the electrode layer below it. Where the taper length was greater than ½ the nominal width of the electrode, that taper length was not applied to that electrode geometry.

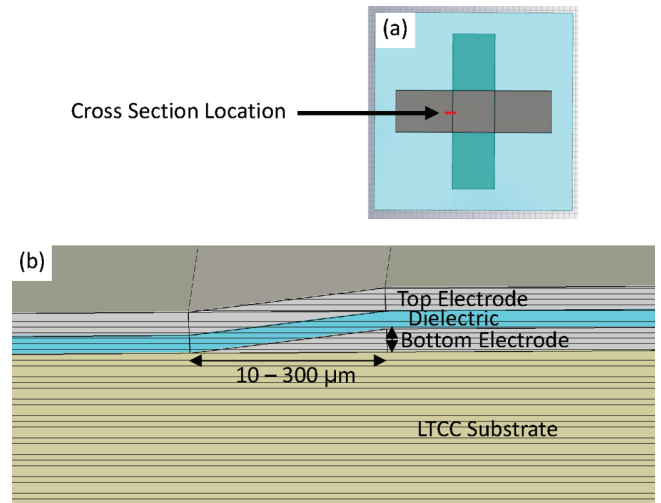


Fig. 4: Model Cross-Section 1 with (a) top view indicating location of the cross-section with red line and (b) showing top electrode and dielectric conform to taper created by bottom electrode.

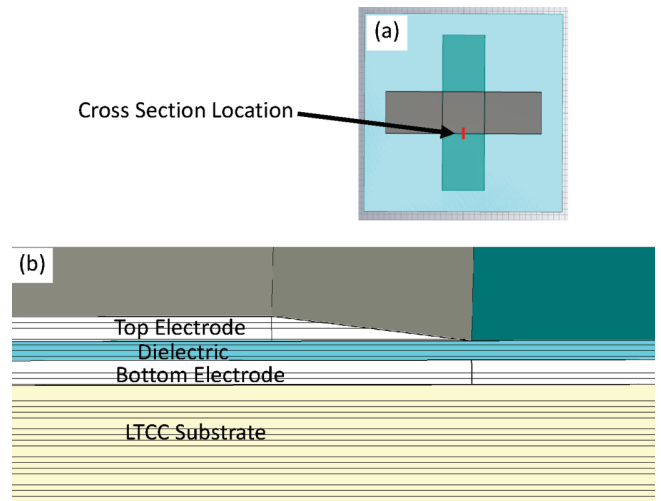


Fig. 5: Model Cross-Section 2 with (a) top view indicating location of the cross-section with red line and (b) showing top electrode with taper over planar dielectric and bottom electrode.

Each of the taper geometry angles was calculated using Eq. 2 and ranged from 0.06 ° to 7.47 ° in this study depending on the electrode and dielectric thickness combination. The model was completely parameterized to allow for a parameter sweep that changed the dielectric thickness, electrode thickness, capacitor width, and capacitor length. Two sets of simulations were performed: one with fringing fields and one without fringing fields. To eliminate fringing fields, magnetic boundary conditions, which force the tangential magnetic field to zero, were placed on the sides of the capacitor. For the simulation with fringing fields, open boundary conditions were used.

$$\text{Angle (degrees)} = \left(\sin^{-1} \frac{t_{\text{electrode}}}{\text{taper}_{\text{length}}} \right) \times \left(\frac{360}{2\pi} \right) \quad (2)$$

A tetrahedral mesh was used for the simulations. The mesh density of the model was increased around the elec-

trode edges as the magnitude of the electric field varied significantly with position near the edges. The finer, more dense mesh near the edges was required for the calculation precision where the field enhancement was significant. Since there was not a field gradient beyond the edge region, a coarser mesh was used, which reduced the complexity of the model without reducing the repeatability of the results. The mesh of the simulation model is shown in Fig. 6 as a top view representation of Fig. 3 looking through the electrode at the meshing of the dielectric layer. The left image of Fig. 6 provides the entire top view of the model's mesh and the right image is an enlarged view showing the mesh detail at the edges.

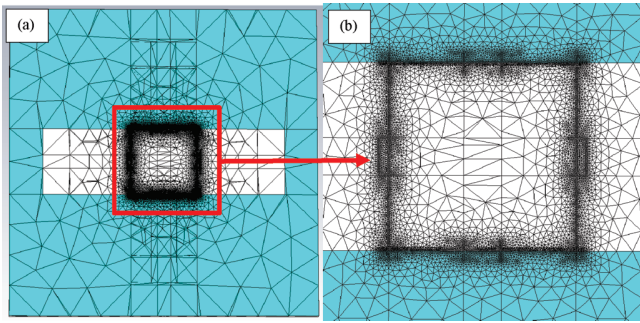


Fig. 6: (a) Tetrahedral mesh of capacitor simulation model. (b) Magnified model showing mesh detail at electrode edges of active capacitor area.

An electric potential was defined on the top electrode while no potential was defined on the bottom electrode. An effective dielectric constant was then calculated by solving the parallel-plate capacitor equation using the capacitance from the simulation.

In these simulations, the behavior for Al_2O_3 was modeled, and amorphous SiO_2 , a lower dielectric constant material ($K = 3.3$), was also modeled. The second material was selected for study because of a possible decrease in the dielectric constant of Al_2O_3 , due to decreased polarizability contributions. Modeling both materials also presented a more complete study of the possible magnitude of fringe field contributions to effective dielectric constant, enabling consideration of device architectures for high-frequency use, as noted earlier.

(3) Calculations of polarizability contributions

As stated above, polarizability contributions of atoms to the dielectric constant may be estimated using the Clausius-Mossotti equation (Eq. 3):

$$\frac{K_e - 1}{K_e + 2} = \frac{1}{3\epsilon_0} \sum_i n_i \alpha_i \quad (3)$$

where K_e is the effective dielectric constant of the material of interest, ϵ_0 is the permittivity of free space (8.85×10^{-12} F/m), n_i is the number of i atoms, and α_i is the polarizability of i atoms. The contributions of the various electronic polarizabilities N_e , ionic polarizabilities N_i , and dipolar polarizabilities N_d can be summed in the Clausius-Mossotti equation in a static electric field and represented with the following equations:

$$\frac{K_e - 1}{K_e + 2} = \frac{1}{3\epsilon_0} (N_e \alpha_e + N_i \alpha_i + N_d \alpha_d) \quad (4)$$

$$\frac{K_e - 1}{K_e + 2} = \frac{4\pi}{3} N_i \alpha_i \quad (5)$$

Eq. 5 can be rewritten to solve for the predicted K_e when the dielectric constant of the material is unknown, for example, as would be the case for amorphous Al_2O_3 :

$$K_e = \frac{\frac{8\pi}{3} N_i \alpha_i + 1}{1 - \frac{4\pi}{3} N_i \alpha_i} \quad (6)$$

By performing calculations with the reported polarizabilities of Al and O, possible effects of material structure/density on the dielectric constant may be analyzed. The results of these calculations were compared with the results reported by Shannon and coworkers⁹, to evaluate contributions to the apparent dielectric constant.

(4) Estimation of accumulation or inversion layer depth

For a metal:dielectric interface, the solution to Poisson's equation yields the penetration depth, x (m) of band bending and therefore an estimate of accumulation or inversion layer depth as:

$$x = \sqrt{\frac{2\epsilon_0 K \Delta\Phi}{qN}} \quad (7)$$

where $\Delta\Phi$ is the difference in work function (J), q is the charge on an electron (1.6×10^{-19} C), and N is the carrier concentration ($\#/m^3$). If the work function of the metal is less than that of the dielectric, electrons are transferred into the dielectric to equilibrate the Fermi levels and an accumulation layer forms. Note the lack of any extrinsic doping yields a low N for an insulating dielectric such as Al_2O_3 , potentially resulting in a significant accumulation or inversion layer depth. Other work within our group¹¹ has shown that for some metals, notably Pt, all thin film capacitor structures were rendered semiconducting and hence inoperable as a capacitor.

III. Results and Discussion

(1) Experimental measurements

Samples were fabricated and measured across 1 kHz to 100 kHz for capacitance and dielectric loss. The capacitors were fabricated on DuPont 951[®] LTCC. As seen in Fig. 7, the capacitance at 1 kHz increased with increasing area, as expected, although the calculated dielectric constant for these samples increased with decreasing area, from a value of approximately 12 to a value of 23 for the smallest devices. The results at 10 kHz and 100 kHz were similar to those shown here at 1 kHz.

(2) Model calculations

CST Studio Suite solves for the electric field (E) and the electric flux density (D) through the structure. Various post-processing steps can be performed, which include the generation of cross-sections of the 3D fields and evaluation of the field strength along the length of the path or electrode in this case. Fig. 8 shows the electric field enhancement at the edge of the electrode. To obtain the effect of the electric field enhancement at the edge of an electrode, the electric field strength was evaluated on a curve across the width of the capacitor.

Various parameters were evaluated using the fringe field model, including electrode thickness, dielectric thickness, and capacitor length and width for the cases with and without fringing. The model predicts a strong dependence of the dielectric constant enhancement due to the fringe field on the capacitor size, as seen in Fig. 9. For the amorphous alumina dielectric, the field enhanced dielectric constant increased by 9%, from 9.9 to 10.7, when the capacitor area decreased from 0.5625 to 0.0225 mm² in this material. For comparison, the fringe field contributed to an increase in the effective dielectric constant of amorphous SiO₂ by 16% using the same experimental parameters, and assuming a bulk dielectric constant of 3.3. This general trend agrees with the observed experimental results shown in Fig. 7.

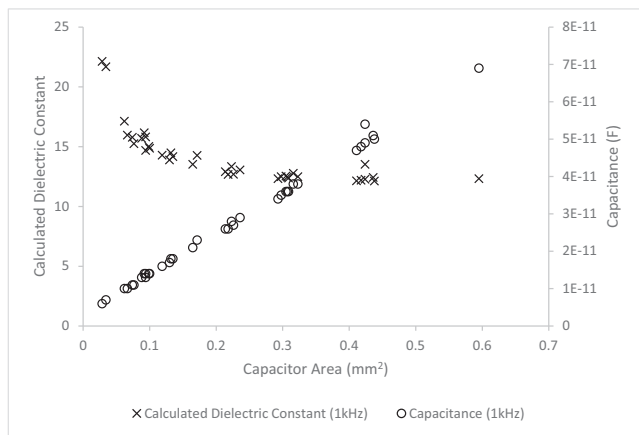


Fig. 7: Dielectric constant and capacitance vs. active dielectric area for Al-Al₂O₃-Al capacitors on LTCC substrate.

The dielectric thickness also had an effect on the enhancement in the dielectric constant. Fig. 10 shows that thicker dielectric devices, e.g. devices with lower capacitance, had a stronger enhancement response compared to thinner dielectric devices.

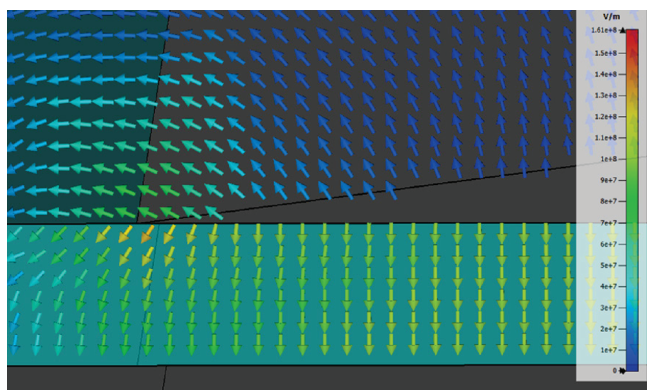


Fig. 8: 2D cross-section of electric field at electrode edge.

(3) Polarizability contributions

Crystalline Al₂O₃ with ideal lattice parameters has a predicted dielectric constant of 10 using the Clausius-Mossotti relationship. There would be no dipolar contri-

butions to the dielectric constant with Al₂O₃ due to the nature of the material. Hexagonal crystalline Al₂O₃ has a theoretical density of approximately 3.98 g/cm³. In contrast, the density of amorphous Al₂O₃ thin films has been reported to be 2.9–3.3 g/cm³, which suggests a free volume of 19–37% greater compared to the crystalline material^{12,13}.

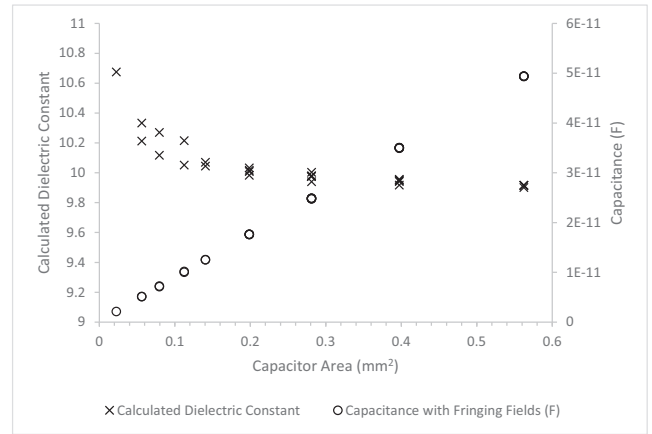


Fig. 9: Model results for dielectric constant and capacitance vs. active dielectric area for Al-Al₂O₃-Al capacitors.

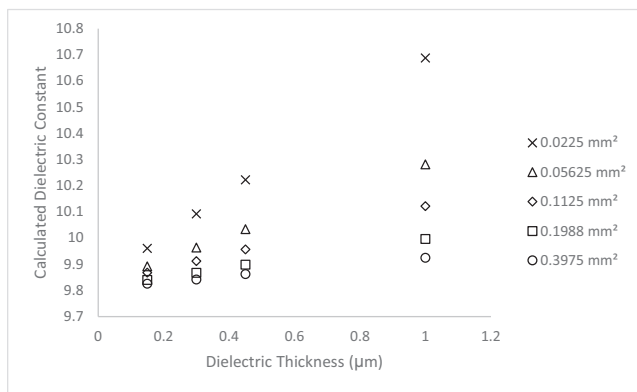
The Clausius-Mossotti relationship from Eq. 6 was used to calculate the dielectric constant for hexagonal Al₂O₃ assuming the standard (crystalline) and expanded (amorphous) interatomic spacing parameters in Table 1. The associated dielectric constant of amorphous Al₂O₃ based on an increased interatomic spacing comparative to densities as low as 3.3–2.9 g/cm³ ranges from 6.1 to 4.6, respectively. From this analysis, polarizability contributions might not be expected to contribute to the enhanced dielectric constants that are observed; in fact, they might be expected to decrease the effective dielectric constant of the films.

While this approach seems to provide a straightforward method to estimate polarizability contributions, it may be too simplistic: the effects of film density have been accounted for, but the role of film structure (atomic arrangement and structural openness) on the polarizability of the species in the film has been neglected. The work of Shannon and colleagues⁹ seems to suggest the polarizability of the Al and/or O species is increased in the amorphous state. Such an increase could reduce, or potentially even eliminate, the expected reduction in dielectric constant predicted by the Clausius-Mossotti equation and the lower density of the amorphous state.

There is one other factor here that should be considered. It has been demonstrated above in the analysis of fringe field contributions to dielectric constant enhancement that such contributions increase with decreasing dielectric constant (9% enhancement for Al₂O₃, K = 9.8; 16% enhancement for SiO₂, K = 3.3). So, if the predictions of the Clausius-Mossotti equation shown in Table 1 are correct, i.e. films with lower density have a lower dielectric constant, such films should demonstrate a greater increase in capacitance due to fringe fields.

Table 1: Clausius-Mossotti-based dielectric constant calculations for hexagonal Al₂O₃ having expanded lattice parameters.

Interatomic Spacing Increase	a (Å)	c (Å)	Calculated Dielectric Constant	Calculated Volume (Å ³)	Calculated Vol % Increase	Calculated Density (g/cm ³)
0%	4.76	12.99	10.00	255.02	0.0%	3.98
1%	4.81	13.12	9.03	262.74	3.0%	3.87
2%	4.86	13.25	8.23	270.63	6.1%	3.76
3%	4.90	13.38	7.56	278.66	9.3%	3.65
4%	4.95	13.51	7.00	286.86	12.5%	3.54
5%	5.00	13.64	6.52	295.21	15.8%	3.44
6%	5.05	13.77	6.10	303.73	19.1%	3.35
7%	5.09	13.90	5.74	312.41	22.5%	3.25
8%	5.14	14.03	5.41	321.25	26.0%	3.16
9%	5.19	14.16	5.13	330.25	29.5%	3.08
10%	5.24	14.29	4.87	339.43	33.1%	2.99
11%	5.28	14.42	4.64	348.77	36.8%	2.91
12%	5.33	14.55	4.44	358.28	40.5%	2.84

**Fig. 10:** Model results of the dependence of the effective dielectric constant on the dielectric thickness for Al-Al₂O₃-Al capacitors with various areas (averages of model results displayed).

Because of the concomitant but potentially competing effects of density on polarizability and fringe field contributions, predicting the magnitude of these effects is difficult. Based on the calculations, it may be tempting to state that polarizability contributions decrease, rather than enhance, the observed dielectric constant. However, it is not possible to unequivocally state this, because of the uncertainty of changes in the magnitude of the fringe field contributions and any potential increase in polarizability due to greater structural free volume. Further experimentation to better quantify the polarizability of the Al and O species in these films is required. While density measurements might provide some insight, they are insufficient to clarify the nature of the polarizability.

(4) Accumulation or inversion layer contributions

Modeling efforts of accumulation or inversion layers are limited since the carrier concentration for Al₂O₃ is unknown. Current-voltage measurements on these devices using an HP4140 picoammeter and an applied potential of

100 V yield current measurements were below the noise level of 10⁻¹³ amps. If the intrinsic reaction is assumed to control conduction, the band gap of Al₂O₃ of ≈ 7 eV yields a calculated carrier concentration at room temperature of ≈ 10⁻³²/m³, a negligible number. While certainly these values are desirable for a capacitor dielectric, the question remains if thin dielectrics are adversely affected. For instance, using $N = 10^4/\text{m}$, $K = 10$ and $\Delta\Phi = 1 \text{ eV}$, as an example, the penetration depth using Eq. 7 calculates to be 133 nm at each electrode, a number that when compared to the dielectric thickness of 1 000 nm would yield an observed capacitance 27 % higher than expected. Band bending of this magnitude might, therefore, decrease the effective thickness of the dielectric, contributing to higher calculated dielectric constants. This effect is being further explored by varying the electrode composition and measuring the capacitor performance at elevated temperatures and field levels.

IV. Conclusions

Thin-film Al-Al₂O₃-Al capacitors on LTCC were fabricated and characterized to have higher than predicted capacitance. The measured capacitance was nearly double the predicted value in some cases. Fringe field, Clausius-Mossotti polarizability, and accumulation layer contributions to capacitance were modeled for this system as potential sources of increased capacitance through dielectric enhancement. Fringe field enhancement to the dielectric constant was successfully modeled using CST Microwave Studio's electrostatic solver and demonstrated up to a 9 % increase in the dielectric constant due to fringe enhancements when a tapered electrode was present. While the fringe field model does not account for the entire dielectric enhancement observed experimentally, it does indicate a trend of increasing dielectric enhancement as the capacitor size decreases, as observed experimentally.

The polarizability modeling that was carried out was inconclusive due to competing effects of density on effective dielectric constant (Clausius-Mossotti calculations), and uncertainty in the polarizability of the species as a function of the free volume of the amorphous structure. Polarizability effects and density can also be expected to affect fringe field contributions, making the analysis of these effects on dielectric constant enhancements even more difficult.

Another likely contribution to the dielectric enhancement of the thin film dielectrics in this study is the reduced effective dielectric thickness arising from accumulation layers in the dielectric adjacent to the electrodes. This contribution has been calculated to increase the capacitance by as much as 27 % based on assumptions documented in this paper. Electron-beam-induced current (EBIC) is being used to characterize the cross-section of these samples for evidence of accumulation layers and their respective reduction of the effective dielectric thickness if present.

Acknowledgments

The submitted manuscript has been authored by a contractor of the U.S. Government under contract no. DE-NA-0002839. Accordingly, the U.S. Government retains a nonexclusive, royalty-free license to publish or reproduce the published form of this contribution or allow others to do so for U.S. Government purposes.

References

- 1 Murray, J., Huebner, W., O'Keefe, M.J., Wilder, K., Etinger, R., Kuhn, W., Krueger, D.S., Wolf, J.A.: Sputter deposition of thin film capacitors on LTCC substrates for RF bypass and filtering applications. In: Proc. of the 44th Int. Symp. on Microelectronics. Long Beach, CA, 2011.
- 2 Wolf, A., Peterson, K., O'Keefe, M., Huebner, W., Kuhn, B.: Fully integrated applications of thin films on low temperature cofired ceramic (LTCC). In: Proc. IMAPS/ACerS 8th Int. CI-CMT Conf. and Exhi. Erfurt, Germany, 2012.
- 3 Kim, C., Senior, D.E., Shorey, A., Kim, H.J., Thomas, W., Yoon, Y.K.: Through-glass interposer integrated high quality RF components. In: Proc. of Electronic Comp. & Technol. Conf., Orlando, FL, 2014.
- 4 Trinh, H.V., Devoe, A.: High voltage fringe-effect capacitor. U.S. Patent 9,786,437, (2017)
- 5 Pillai, K.P.P.: Fringing fields in finite parallel-plate capacitors. In: Proc. Inst. of Electrical Eng. London, England, 1970.
- 6 Naini, A., Green, M.: Fringing fields in parallel-plate capacitor, *Am. J. Phys.*, **45**, 877–879, (1977).
- 7 Chen, P., Liu, J., Zhang, H., Chu, B.: Increase of capacitance of thick dielectrics by fringe effect, *IEEE T. Dielectr. Electr. Insul.*, **26**, 1716–1719, (2019).
- 8 Subramanian, M.A., Shannon, R.D., Chai, B.H.T, Abraham, M.M., Wintersgill, M.C.: Dielectric constants of BeO, MgO, and CaO using the two-terminal method, *Phys. Chem. Miner.*, **16**, 741–746, (1989).
- 9 Shannon, R.D., Dickinson, J.E., Rossman, G.R.: Dielectric constants of crystalline and amorphous spodumene, anorthite and diopside and the oxide additivity rule, *Phys. Chem. Miner.*, **19**, 148–156, (1992).
- 10 Kuhn, W.B., Fund, A.D., Wolf, J.A., Schwartz, R.W., Claypool, J., O'Keefe, M.J., Huebner, W.: Thin film capacitor technology for improving power integrity, *IEEE T. Comp. Pack. Man.*, **9**, 1319–1327, (2019).
- 11 Krueger, D.S.: Contributions to the performance of thin film capacitors for high reliability applications, doctoral dissertation, Missouri University of Science and Technology, ProQuest Dissertations Publishing, (2021)
- 12 Tane, M., Nakano, S., Nakamura, R., Ogi, H., Ishimaru, M., Kimizuka, H., Nakajima, H.: Nanovoid formation by change in amorphous structure through the annealing of amorphous Al₂O₃ thin films, *Acta Mater.*, **59**, 4631–4640, (2011).
- 13 Etinger-Geller, Y., Katsman, A., Pokroy, B.: Density of nanometrically thin amorphous films varies by thickness, *Chem. Mater.*, **29**, 4912–4919, (2017).

